1 Introduction

A linear polymer, or macromolecule, is a long molecule formed by monomers joined in a sequence by covalent bonds. The structural properties of macromolecule depends on the system state. In good solvent, there is excluded volume effect and polymer is in denatured, or unfolded, regime. Globular, or collapsed, phase corresponds to polymer immersed in poor solvent. In the critical point, the phase space is divided into two regions corresponding to open and globular states of polymer [1].

Coarse-grained models of macromolecules are widely used for macromolecular modeling. In these models, polymers are represented using subunits which are formed by groups of atoms instead of individual atoms (see Chap.1 in Ref.[2]). Such models neglect chemical details. As coarse-grained models decrease the number of degrees of freedom, it is convenient approach to simulate systems to obtain statistical properties.

The simplest model of polymer is classical homopolymer model which is represented by interacting (also known as collapsing) self-avoiding walk (SAW). This is well-studied model, including cases for different lattices (see Ref.[1, 3]). Self-avoiding walks allows to include excluded volume effects for polymers in good solvent. Van der Waals type attraction is modeled via including the nearest neighbor monomer attraction. Critical phenomena take place in the infinite systems in second order phase transition which is defined as a singularity of free-energy function (see Chap.3 in Ref [4]).

In homopolymer model, all monomers are the same. The polymers with different types of subunits are called heteropolymers. The simplest heteropolymer model is Hydrophobic-polar (HP) model of protein [5]. It assumes that the sequence of monomers types are fixed. This model was introduced to approximate the folding process of protein and mostly used for development algorithms to find minimum energy states (for example, [6, 7]). This model also was used to explore conformations space of proteins [8]. We studied the case of dynamical HP model where sequence of monomers and geometry structure are not fixed [9]. Computational results do not contradict the assumption that dynamical HP model and an interacting homopolymer have the similar behavior in phase transition point and they are in the same universality class.

To represent the ferromagnetic properties of material, the Ising model was introduced. The 2D square-lattice Ising model is the simplest example of system which undergoes a phase transition between ordered states. To study magnetic polymers, Garel et.al introduced the Ising model on self-avoiding walks [10] and studied it for 2D and 3D lattices [10, 11]. After, this model was studied more [12, 13]. Computational results show that the system has second-order transition in 2D case and first-order transition on 3D lattice.

In this work, we continue to study magnetic polymer. We study XY model on SAWs for 2D lattice. Classical XY model on 2D square lattice has a topological order, which was proposed theoretically and named Kosterlitz-Thouless (KT) phase transition [14]. After, classical 2D was studied numerically using Monte-Carlo methods [15, 16].

2 Models

2.1 XY model on self-avoiding walks (SAWs)

A molecular conformation of the length N is represented by a self-avoiding walk (SAW) on a regular lattice with $N - 1$ edges and N nodes. Each ith node represents a spin-like variable s_i which is associated with angle $\theta_i \in [-\pi; \pi]$. The Hamiltonian for sequence of spins s and conformation u is defined as the sum over all non-repeating neighbor pairs $\langle i, j \rangle$ in conformation:

$$H(u,s) = -J \sum_{\langle i,j \rangle} cos(\theta_i - \theta_j) - h \sum_i cos(\theta_i) \tag{2.1}$$

In case of the free boundary conditions, the partition function for the chain of the length N has the following form:

$$Z(J) = \int_{-\pi}^{\pi} d\theta_1 d\theta_2 \ldots d\theta_N e^{J(cos\theta_1 - \theta_2)} e^{J(cos\theta_2 - \theta_3)} e^{J(cos\theta_{N-1} - \theta_N)} \tag{2.2}$$

The mean magnetization is defined as a vector:

$$\langle m \rangle = \frac{1}{N} \langle (\sum_{i=1}^{N} cos\theta_i, \sum_{i=1}^{N} sin\theta_i) \rangle \tag{2.3}$$

The second moment of magnetization is a square of the norm:

$$\langle m^2 \rangle = \frac{1}{N^2} \langle (\sum_{i=1}^{N} cos\theta_i)^2 + (\sum_{i=1}^{N} sin\theta_i)^2 \rangle \tag{2.4}$$

From measurements of the average magnetization per spin $\langle m \rangle (J)$, we can obtain the value of the magnetic cumulant (Binder parameters) of fourth order [17], which is helpful to study magnetic phase transition:

$$U_4(J) = 1 - \frac{\langle m^4 \rangle}{3 \langle m^2 \rangle^2} \tag{2.5}$$

2.1.1 Case without interaction (J=0)

In case $J = 0$ (high-temperature regime), all states have equal probabilities:

$$Z(0) = \int_{-\pi}^{\pi} (\frac{1}{2\pi})^N d\theta_1 d\theta_2 \ldots d\theta_N \tag{2.6}$$

To calculate the exact value of $\langle m^2 \rangle (J = 0)$ we use following results:

$$\int_{-\pi}^{\pi} \frac{1}{2\pi} sin^2\theta d\theta = \int_{-\pi}^{\pi} \frac{1}{2\pi} cos^2\theta d\theta = \frac{1}{2}$$

$$\int_{-\pi}^{\pi} \frac{1}{2\pi} sin\theta d\theta = \int_{-\pi}^{\pi} \frac{1}{2\pi} cos\theta d\theta = 0$$

After some calculation, only integration results for N times $sin^2\theta_i$ and N times $cos^2\theta_i$ survive:

$$\langle m^2\rangle(J=0) = \frac{1}{N^2}\int_{-\pi}^{\pi}(\frac{1}{2\pi})^N\left((\sum_{i=1}^{N}cos\theta_i)^2 + (\sum_{i=1}^{N}sin\theta_i)^2\right)d\theta_1 d\theta_2\ldots d\theta_N = \frac{1}{N^2}(\frac{1}{2}N + \frac{1}{2}N) = \frac{1}{N} \quad (2.7)$$

Next, to calculate $\langle m^4\rangle(J=0)$ we use following facts:

$$\langle m^4\rangle(J=0) = \frac{1}{N^4}\int_{-\pi}^{\pi}(\frac{1}{2\pi})^N\left((\sum_{i=1}^{N}cos\theta_i)^2 + (\sum_{i=1}^{N}sin\theta_i)^2\right)^2 d\theta_1 d\theta_2\ldots d\theta_N$$

$$\left((\sum_{i=1}^{N}cos\theta_i)^2 + (\sum_{i=1}^{N}sin\theta_i)^2\right)^2 = (\sum_{i=1}^{N}cos\theta_i)^4 + (\sum_{i=1}^{N}sin\theta_i)^4 + 2(\sum_{i=1}^{N}cos\theta_i)^2(\sum_{i=1}^{N}sin\theta_i)^2$$

$\int_{-\pi}^{\pi}\frac{1}{2\pi}sin^4\theta d\theta = \int_{-\pi}^{\pi}\frac{1}{2\pi}cos^4\theta d\theta = \frac{3}{8}$ (We have N times $sin^4\theta_i$-term and N times $cos^4\theta_i$-term what results in $2\times\frac{3}{8}\times N$).

$\int_{-\pi}^{\pi}\frac{1}{2\pi}\int_{-\pi}^{\pi}\frac{1}{2\pi}sin^2\theta_i sin^2\theta_j d\theta_i d\theta_j = \int_{-\pi}^{\pi}\frac{1}{2\pi}\int_{-\pi}^{\pi}\frac{1}{2\pi}cos^2\theta_i cos^2\theta_j d\theta_i d\theta_j = \frac{1}{4}$ (We have $6N(N-1)\frac{1}{2}$ times sin-term and $6N(N-1)\frac{1}{2}$ times cos-term what results in $6\times\frac{1}{4}\times N(N-1)$).

$\int_{-\pi}^{\pi}\frac{1}{2\pi}sin^2\theta cos^2\theta d\theta = \frac{1}{8}$ (We have this term $2N$ times what results in $2\times\frac{1}{8}\times N$).

$\int_{-\pi}^{\pi}\frac{1}{2\pi}\int_{-\pi}^{\pi}\frac{1}{2\pi}cos^2\theta_i sin^2\theta_j d\theta_i d\theta_j = \frac{1}{4}$ (We have $2N(N-1)\frac{1}{2}$ times what results in $2\times\frac{1}{4}\times N(N-1)$).

All other terms with odd power of sin of cos function equals zero after integration over period.

$$\langle m^4\rangle(J=0) = \frac{1}{N^4}\left(2\times\frac{3}{8}\times N + 6\times\frac{1}{4}\times N(N-1) + 2\times\frac{1}{8}\times N + 2\times\frac{1}{4}\times N(N-1)\right) = \frac{2N-1}{N^3}$$

$$U_4(J=0) = 1 - \frac{\frac{2N-1}{N^3}}{3\frac{1}{N^2}} = 1 - \frac{2N-1}{3N} = \frac{1}{3} + \frac{1}{3N} \quad (2.8)$$

2.2 Structural properties

To study structural phase transition, we use the mean square end-to-end distance (radius) of self-avoiding-walks which is defined as the sum over all configurations:

$$\langle R_N^2\rangle = \frac{1}{Z_N}\sum_{|u|=N}|u|^2 e^{-E_u}, \quad (2.9)$$

where $|u|$ is the Euclidean distance between the endpoints of conformation u, and Z_N is partition function in the canonical assemble (2.2). As $N\to\infty$, the mean radius of SAWs is believed to scale as

$$\langle R_N^2\rangle \sim N^{2\nu}. \quad (2.10)$$

Here ν is the critical exponent.

2.2.1 The square lattice, 2D

In two dimensions, the exact value for non-interacting SAWs ($J = 0$)[18]

$$\nu = \frac{3}{4}. \tag{2.11}$$

The case of non-interacting SAWs is equivalent to case $J = 0$ for XY model on polymers or Ising model on polymers [13]. Consider collapsing self-avoiding walks, or classical homopolymer model (see chapter 9 in Ref.[1]. For thermodynamic limit $N \to \infty$, ν is believed to have the form of a step function of interaction energy J. For finite systems, this effect is rounded [3]. At low $J < J_\theta$, the system is equivalent to SAW without interaction. At the theta-point, ν_θ is obtained via Coulomb-gas approximations [19]:

$$\nu_\theta = \frac{4}{7}. \tag{2.12}$$

For the globular regime ($J > J_\theta$) in 2D case:

$$\nu = \frac{1}{2}. \tag{2.13}$$

2.2.2 The cubic lattice, 3D

For 3D case, in $J = 0$, the Flory predicted value for self-avoiding walk is following:

$$\nu = \frac{3}{2 + d} = frac35. \tag{2.14}$$

The critical exponent ν was also estimated numerically [18]:

$$\nu = 0.5877 \pm 0.0006. \tag{2.15}$$

At the theta-point, the ν_θ is [1]

$$\nu = \frac{1}{2}. \tag{2.16}$$

For compact regime when $J > J_\theta$, the critical exponent ν has following value:

$$\nu = \frac{1}{3}. \tag{2.17}$$

3 Methods

3.1 Monte-Carlo methods

In this work, we construct Markov Chain Monte Carlo method for fixed-length chain consisting of three types of updates. We refer to them as Snake-like step, Reconnection and Wolff Cluster update. In each iteration, the algorithm chooses the update according to probabilities. We define these probabilities as P_{local}, $P_{reconnect}$ and P_{Wolff} respectively. The sum of probabilities is always equal to one: $P_{local} + P_{reconnect} + P_{Wolff} = 1$.

4 Results

4.1 XY model on SAWs, 2D

To perform MC simulations for short chains from $N = 100$ to $N = 1000$, we run at least 2.1×10^9 MC steps using two types of updates: snake-like and reconnect. We choose following update probabilities: $P_{local} = 0.8$, $P_{reconnect} = 0.2$.

For longer chains $N > 1000$ we additionally use cluster update. For $N = 4900$, we run at least 8×10^{10} MC steps. Here we use these values for update probabilities: $P_{local} = 0.8$, $P_{reconnect} = 0.199$, $P_{Wolff} = 0.001$.

4.1.1 Tests for validation simulations

To test our Monte-Carlo (M) simulation, we compare results obtained using MC and Sampling + Exact Enumeration (EE). The exact numeration is the generation of all self-avoiding walks of the particular low value N using recursion technique. As the space of spin configuration is continuous, we simply sample a lot of vectors which components come from the uniform distribution $U(-\pi, \pi)$. For each generated SAW-conformation we generate the set of spin configurations. This allows to obtain mean values and sum generated sets to the partition function. This method is not reliable, but it helps to make approximate checks.

We calculate Mean Radius (2.9), mean energy (2.1) and second moment of magnetization (2.4) for short chains ($N = 5, N = 8$). The generation of spin configuration and applied it to the whole set of SAWs is resource-consuming procedure. Therefore, we sample spin configurations only 600 times (so, 600 sequences of spins applied to each conformation) and repeat this 10 times. Figure 4.1 shows obtained results. For $J = 0$, the second moment of magnetization are close to exact values (2.7) and the mean energy starts at $\langle e \rangle = 0$.
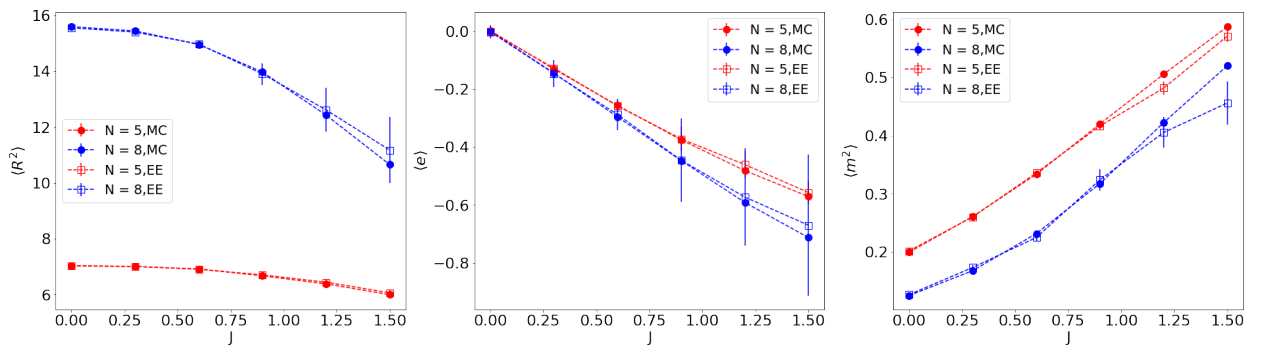

Figure 4.1: $h = 0$. Mean Radius (2.9), mean energy (2.1) and second moment of magnetization (2.4).

4.1.2 Thermodynamic properties

First, we measure the mean square magnetization (2.4) and the mean energy (2.1) for short chains (up to $N = 1000$) in the large range of the interaction energy J and for long chains (up to $N = 4900$) in the narrow range where the system are expected to undergo the phase transition.
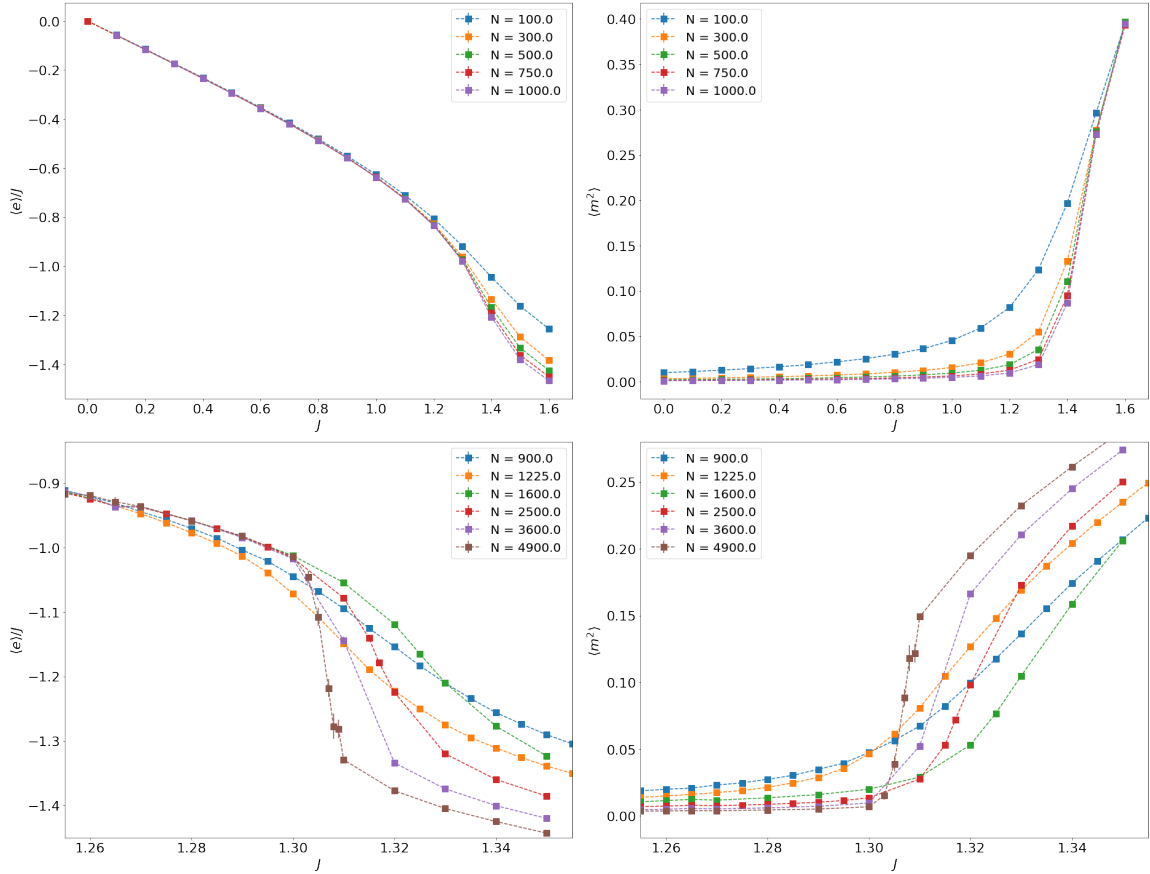
Figure 4.2: $h = 0$. Mean energy (2.1) and second moment of magnetization (2.4).

Figure 4.2 (left column) shows computational results for the mean energy (2.1) as a function of J. At the top plot for short chains, the mean energy starts at $\langle e \rangle = 0$ as expected for unfolded disordered SAWs. As $N \to \infty$, the value of the mean energy decreases and goes to the asymptotic value $\langle e \rangle = -2J$ for compact ordered walk.

Figure 4.2 (right column) illustrates obtained numerical results for the second moment of magnetization (2.4). At $J = 0$, results are consisted with the exact solution (2.7) and $\langle m^2 \rangle \to 0$ as $N \to \infty$. As J increases, the square of magnetization grows up. One can suppose an ordering behavior for large J.

From both energy and the second magnetization moment, we can clearly see the finite size effect. The longer chains has jumps in the function for lower J in comparison to shorter ones.

4.1.3 Structural properties

Next, we estimate critical exponent ν (2.10) from the asymptotic power law for the mean square end-to-end distance of SAWs. We use following ansatz [20]:

$$\log(R_N^2 + k_1) = 2\nu \log(N + k_2) + b. \tag{4.1}$$
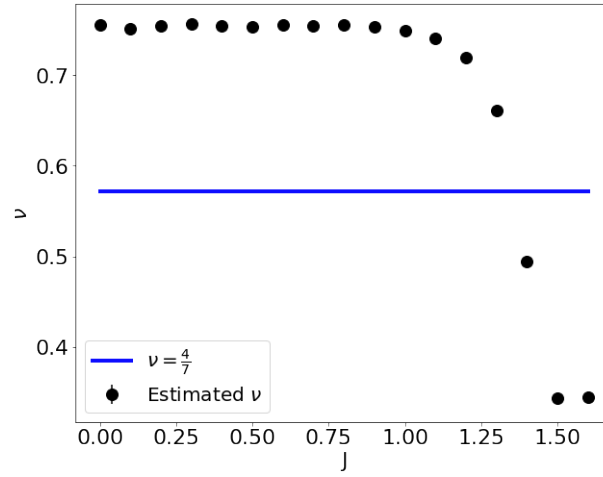
Here $k_1 = k_2 = 1$ are phenomenological parameters.

Figure 4.3: $h = 0$. Estimations with errorbars of critical exponent ν .

For the start, we perform curve-fitting for short chains on the large range of values J. Figure 4.3 illustrates obtained results of exponent estimation. In $J = 0$, the critical exponent ν equals $\nu = \frac{3}{4}$ which is consisted with the value of non-interacting SAWs (2.11). The value $\nu = \frac{4}{7}$, which is the exact value for interacting SAWs (2.12), appears at the region $1.25 < J < 1.4$. In previous section we showed that the energy and second magnetization moment functions of J have jumps approximately at the same region.

We can assume that XY model on SAWs also has value $\nu = 4/7$ (2.12) at the point of structural phase transition. We use this value to obtain collapsing plots in Figure 4.4 in following subsection 4.1.4.

4.1.4 Transition

To focus on studying phase transition, we calculate two characteristics. The first one is the mean square end-to-end distance scaled using the factor $\nu = \frac{4}{7}$ in (2.10). The second one is Binder cumulant of magnetization (2.5). Figure 4.4 presents obtained calculations.
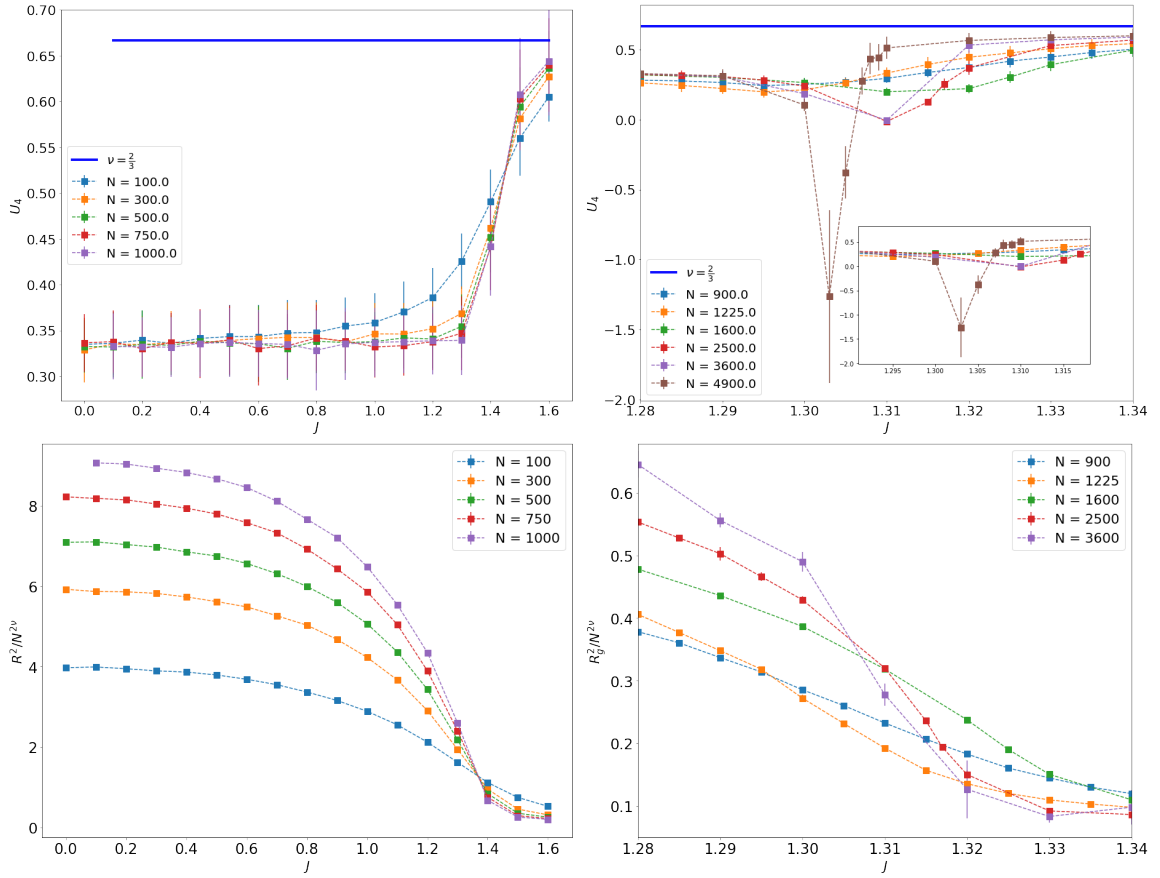
Figure 4.4: $h = 0$. Binder cumulants (2.5) and mean radius (2.9).

The Binder parameter could be used to determine the universality class [21]. At phase transition, the Binder ratio has a divergent feature at the step if the system has the first order transition. Figure 4.4 (top) shows that Binder curves diverge for 2D XY model on SAWs. We can see that in the large systems at the transition region the critical value U_4 is smaller as N larger. Here, we assume that the model undergoes the first order transition and study it further using distribution in Section 4.1.5. The errorbars for curve $N = 4900$ are huge, however, we can narrow the region where the phase transition point is located: $J_{cr} \in [1.29; 1.32]$.

Estimation of $\hat{J}_\theta$

In the bottom of Figure 4.4 we can see that scaled curves of mean radius cross approximately at the same point where long chains have minimum values of Binder cumulant. The right plot also shows us the finite size effect. To make estimation of the critical point, we make following procedure with paired crossings using Monte-Carlo data:

1. Choose the pair of two different N values for length of the chain. Choose the range of values for interaction energy J. This segment should be as short as possible and include the point of intersection of the two curves.

2. For each point from the set generate $n_{samples}$ values using Normal distribution with mean and standard error of $\langle R^2 \rangle / N^{2\nu}$ as parameters: $X_{J,N} \sim N(\langle R^2 \rangle / N^{2\nu}, \sigma(\langle R^2 \rangle / N^{2\nu}))$. We generate for each value J and N 100 samples: $n_{samples} = 100$.

3. Using generated set, for each pair J and N make estimation for mean and standard deviation $\langle R^2 / N^{2\nu}(J, N) \rangle$.

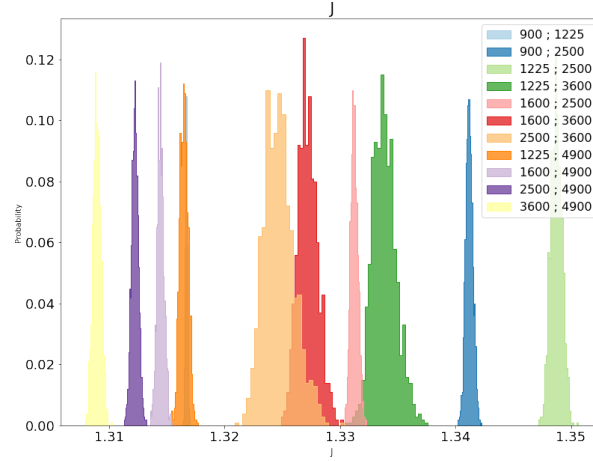4. Apply weighted least squares regression to find crossing point. Save the obtained estimation for $\hat{J}_\theta$.

Figure 4.5: $h = 0$. Histograms of estimated J_θ from paired regressions.

5. Repeat steps 2-5 n_{lines} times. We repeat it $n_{lines} = 1000$ times.

6. At the end, we have n_{lines} of estimated $\hat{J}_\theta$ where two curves cross. This set of obtained estimations is histogram in Figure 4.5.

Histograms for pairs from Figure 4.5 shows us how the size of systems affect the estimations $\hat{J}_\theta$. One way to choose the estimation for phase transition point $\hat{J}_\theta$ in thermodynamic limit is to focus on pairs for long chains such as $N = 3600$ and $N = 4900$. Consider the set of results for $N = 4900$. We have calculations for four pairs $[N_i, 4900]$ which presented in Figure 4.5. We construct the dependence of estimates $\hat{J}_\theta$ on $1/N_i$. Using this measurements, we perform curve-fitting using weighted least squares regression. The fitting results are plotted in Figure 4.6. Estimation of critical point is the point of the limit $1/N_i \to 0$. We obtain the following results:

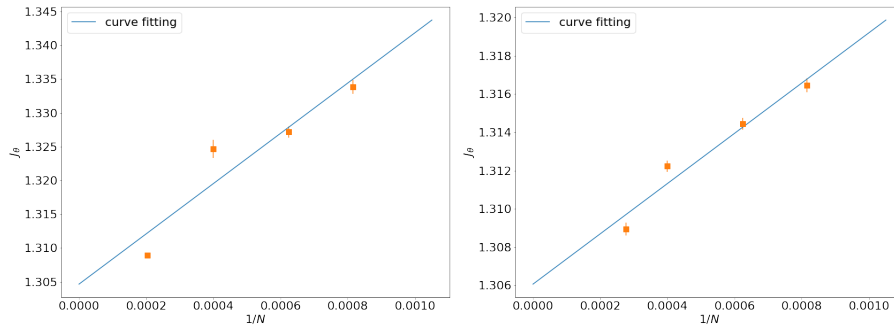$$J_\theta^{3600} \approx 1.3(06); J_\theta^{4900} \approx 1.3(04). \tag{4.2}$$

Figure 4.6: $h = 0$. Pairs with $N = 3600$ (left) and $N = 4900$ (right).

4.1.5 Distribution of $\langle cos\theta \rangle$ and $\langle e \rangle$

To study the phase transition order, we look to distributions of energy and magnetization.

We start our observation of distributions with quite shore chain $N = 1600$. Here (Figure 4.7, top), we notice that energy distribution shape is getting wider around the critical region $J_{cr} \in [1.29; 1.32]$ which was defined using results from Figure 4.4. These curves do not help enough to determine signs of first order transition.

Next, we turn our attention to the longer chains $N = 2500$ (Figure 4.7, medium). In this case, we see broad maybe-bimodal shape of energy distribution at the points $J = 1.317$ and $J = 1.32$.

Finally, we investigate the Monte-Carlo results for $N = 4900$ (Figure 4.7, bottom). The curve of the energy distribution obtained for simulation in $J = 1.307$ is bimodal which corresponds to the first-order phase transition.
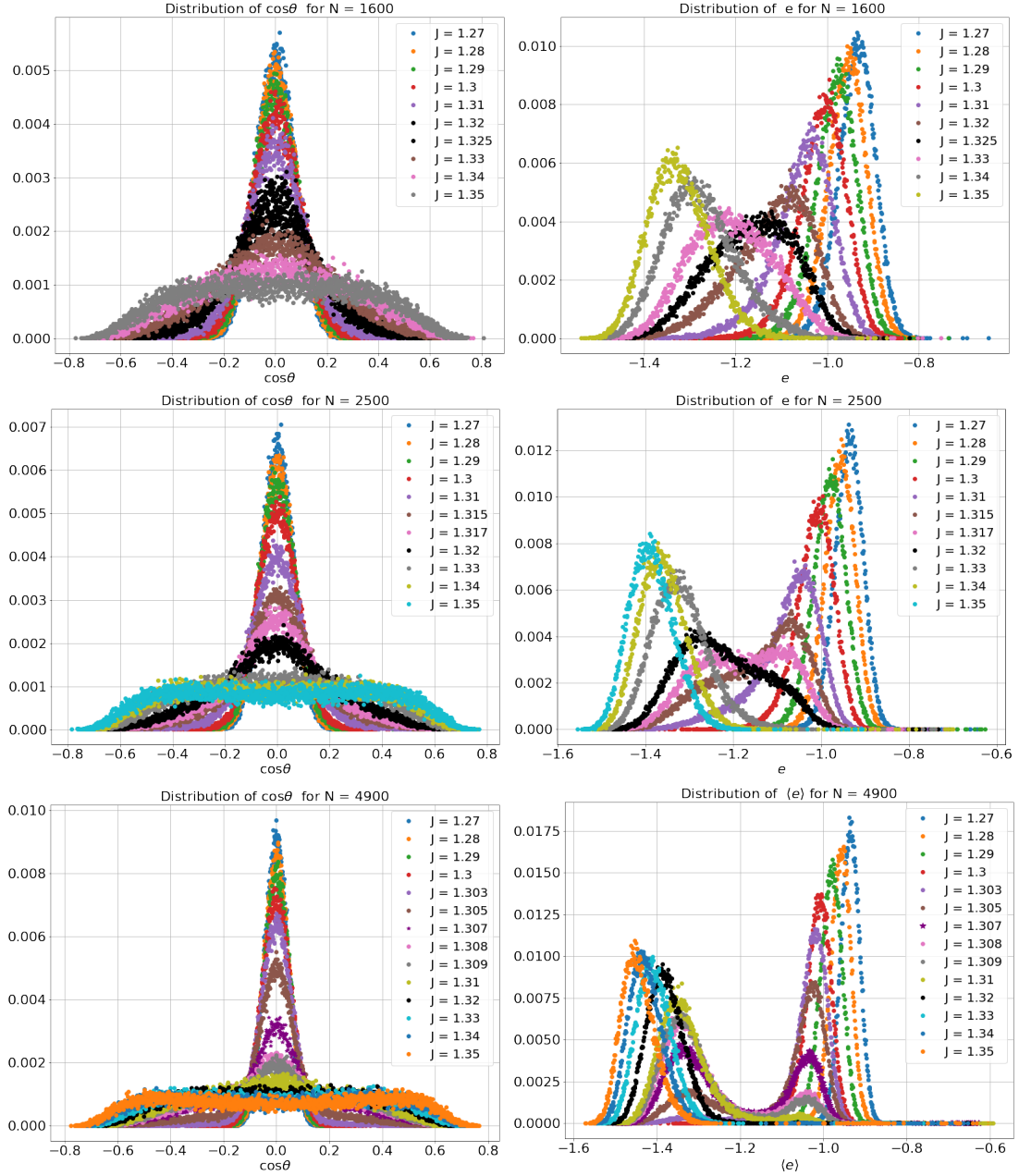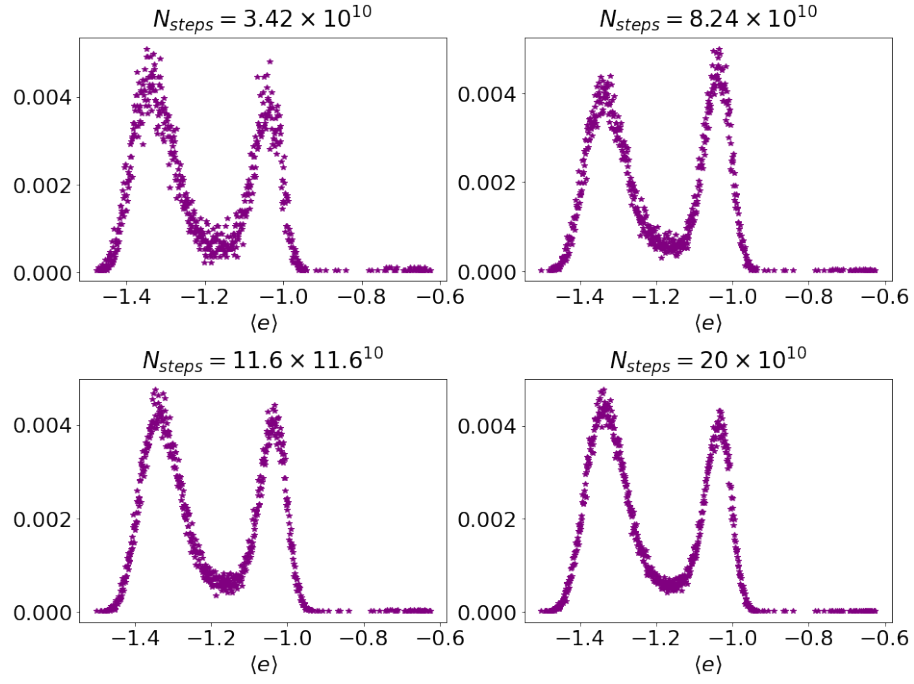

Figure 4.7: $h = 0$.

To examine that shape of the energy critical distribution is truly bimodal, we monitor the curve over simulation and fix four phase of the simulation in Figure 4.8. We see that the results at the beginning are quite noisy, however, the data converge to bimodal shape. Here, we can make an estimation $J_\theta \approx 1.3(0)$ as we obtain bimodal plot at the point $J = 1.307$.

Figure 4.8: $h = 0$.

We also observe the distributions of $\langle cos\theta \rangle$ as a magnetic property. We notice that over the critical region the shapes of distributions are far from Normal-like curves and have signs of phase coexistence. **foster ?**
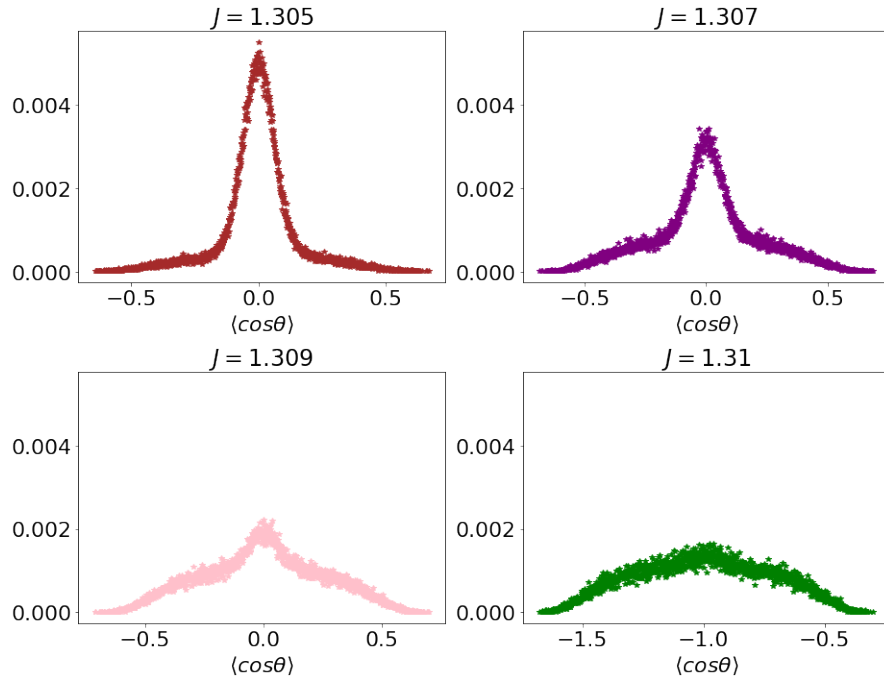
Figure 4.9: $h = 0$.

4.1.6 Summary for 2D case

We study XY model on self-avoiding walks on the square lattice (2D case) using Monte-Carlo simulations. In this work, we consider regime when both conformations and spins are dynamic. Our computational results are consistent with assumption that such model has first-order transition at the critical point.
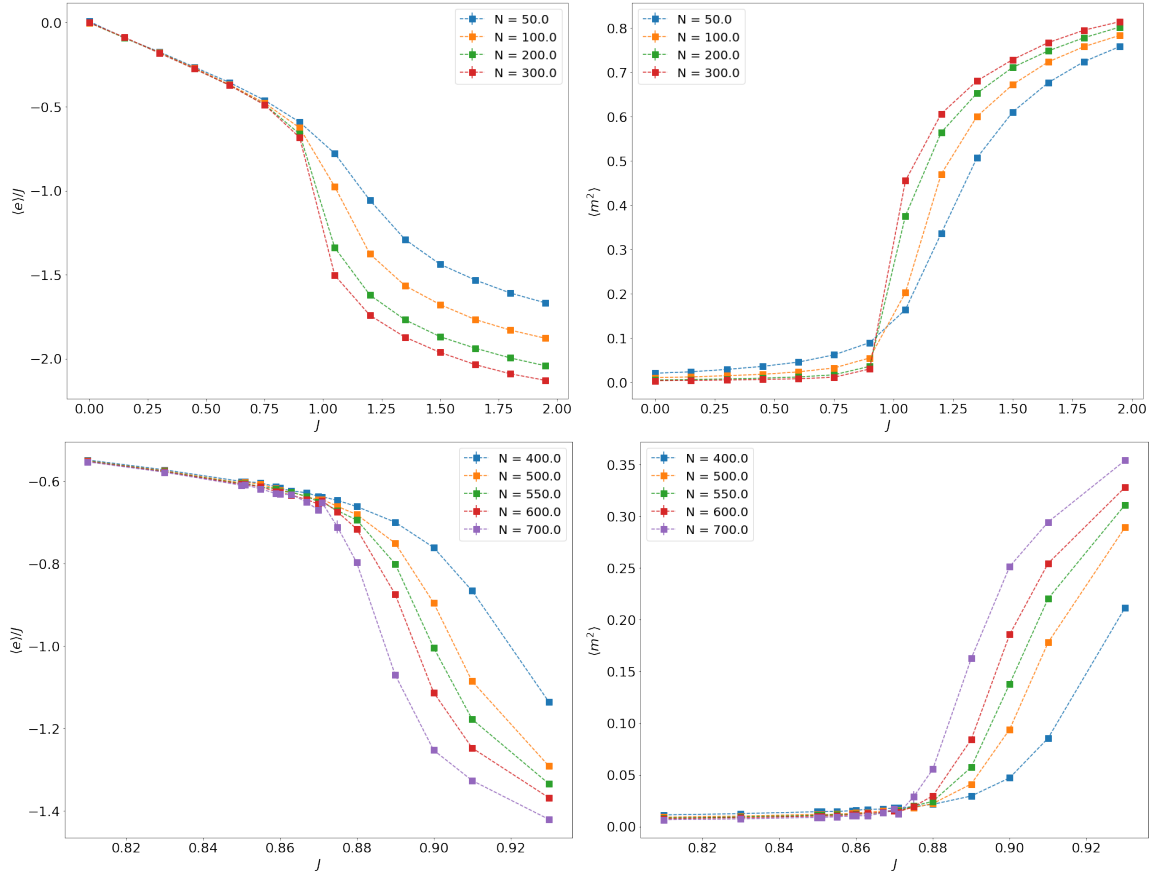
Figure 4.10: $h = 0$. Mean energy (2.1) and second moment of magnetization (2.4).

4.2 XY model on SAWs, 3D

Here, we we study XY-model on SAWs on the cubic lattice. The sequence of our actions is similar to investigation of 2D case.

We make short MCMC simulations for short chains from $N = 50$ to $N = 300$ to narrow the region of critical behavior. MC steps. We use following values for update probabilities: $P_{local} = 0.8$, $P_{reconnect} = 0.199$, $P_{Wolff} = 0.001$. For $N = 300$, we run at least 1.6×10^9 algorithm iterations.

For longer chains from $N = 400$ to $N = 700$ we use these values for update probabilities in the algorithm: $P_{local} = 0.5$, $P_{reconnect} = 0.4$, $P_{Wolff} = 0.1$. We run at least 2×10^{10} MC steps for $N = 700$.

4.2.1 Thermodynamic properties

Again, wee measure the mean square magnetization (2.4) and the mean energy (2.1) to superficially investigate the system.

The squared magnetization (right column in Figure 4.10) grows up as the interaction energy J increases. This behavior is similar to 2D case.

The mean energy (left column in Figure 4.10) tends to get lower for low-temperature regime which could be a sign of compact ordered phase.

From curves of both properties mean squared magnetization and mean energy, we can assume that the critical point is in the interval $J_\theta \in [0.84; 0.92]$.

4.2.2 Structural properties

Here we use the procedure from 4.1.3 to test the hypothesis that the critical exponent ν takes the proposed critical value (2.16) at the approximated critical region $J_\theta \in [0.84; 0.92]$.
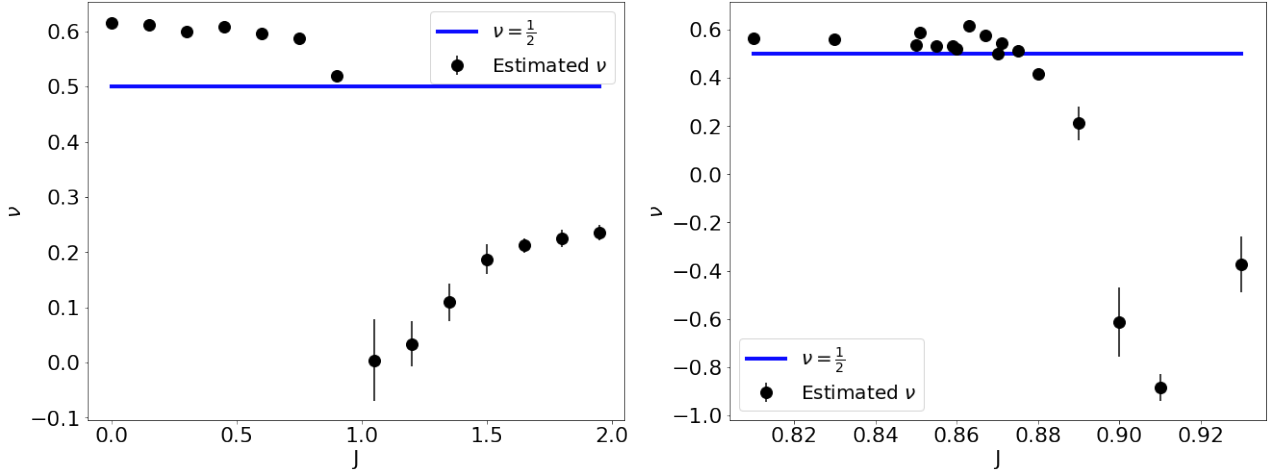

Figure 4.11: $h = 0$. Estimations with errorbars of critical exponent ν .

Figure 4.11 illustrates the obtained results for ν estimations. In the non-interacting regime, we get $\nu \approx 0.6(1)$ for the short chains from $N = 50$ to $N = 300$. This results is close to Flory prediction (2.14). We also see that the possible critical value (2.16) appears approximately at the region $J_\theta \in [0.84; 0.92]$. We use $\nu = \frac{1}{2}$ as the critical exponent for the further study.
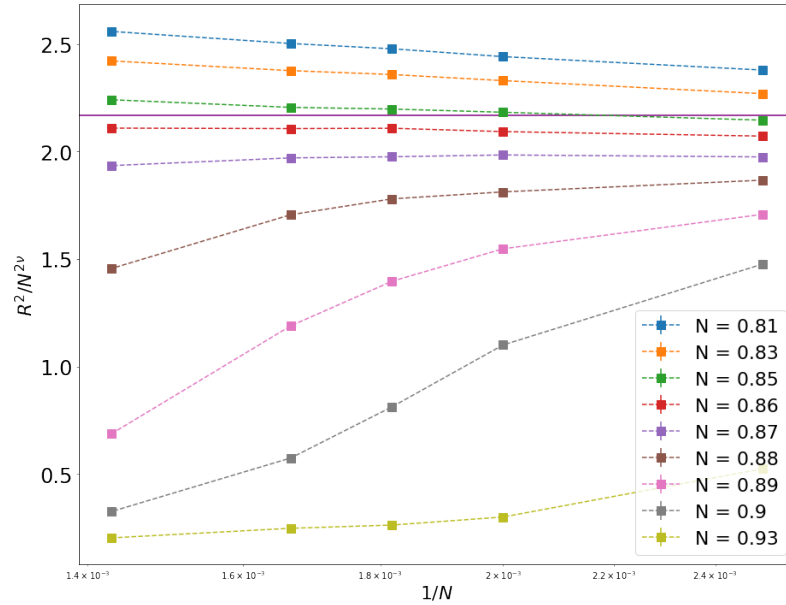

Figure 4.12: $h = 0$. Scaled Mean-squared end-to-end distance using $\nu = 1/2$ as a function of $1/N$.

4.2.3 Transition

To investigate the critical behavior at the phase transition, we again collate the Binder cumulants values (2.5) and scaled mean end-to-end distance (2.9).
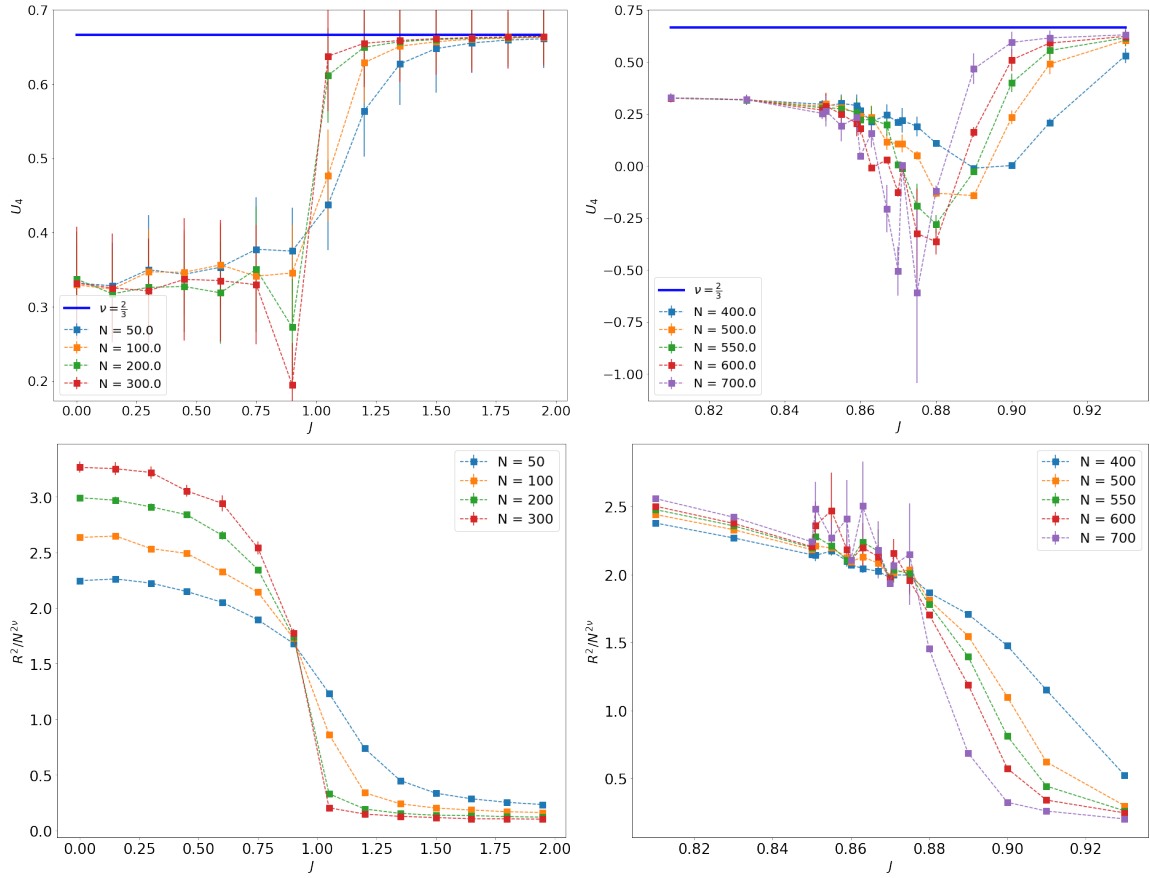
Figure 4.13: $h = 0$. Binder cumulants (2.5) and mean radius (2.9). The mean radius is scaled by $\nu\,frac12$.

The Binder parameters curves (top Figure 4.13) diverges at the critical region similar to XY on SAWs on the square lattice. This is sign of the first-order phase transition. We check the distributions of thermodynamic characteristics in subsection 4.2.4.

The scaled curves of the end-to-end distance cross at the region where Binder cumulants diverge. We can estimate the critical value of the interaction energy J repeating the procedure described in the 4.1.4. Figure 4.14 shows us histograms for paired crosses.

The fitting results are plotted in Figure 4.15. Estimation of critical point is the point of the limit $1/N_i \to 0$. We obtain the following value:

$$J_\theta^{700} \approx \tag{4.3}$$

4.2.4 Distribution of $\langle cos\theta \rangle$ and $\langle e \rangle$

In the subsection 4.2.3 we assumed that XY model on SAWs has first-order phase transition according to the divergence of the Binder cumulants. Now we look to the distribution of the energy and magnetization component to study it further.
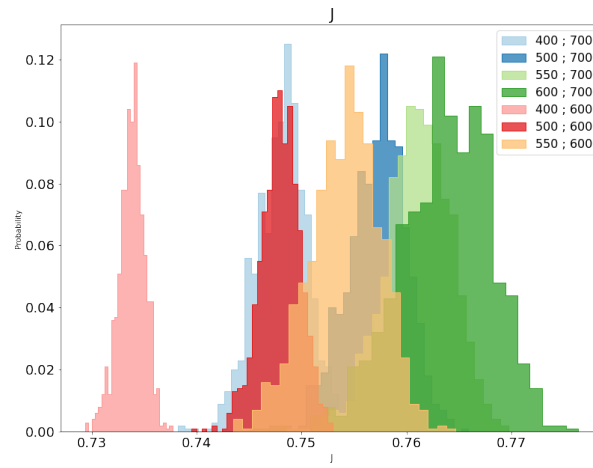
Figure 4.14: $h = 0$. Histograms of estimated J_θ from paired regressions.
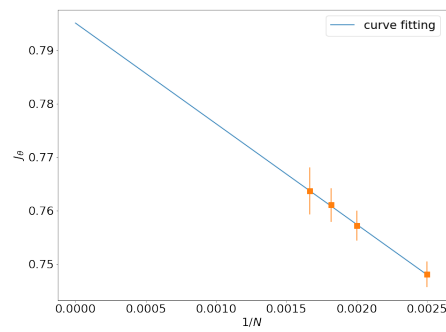

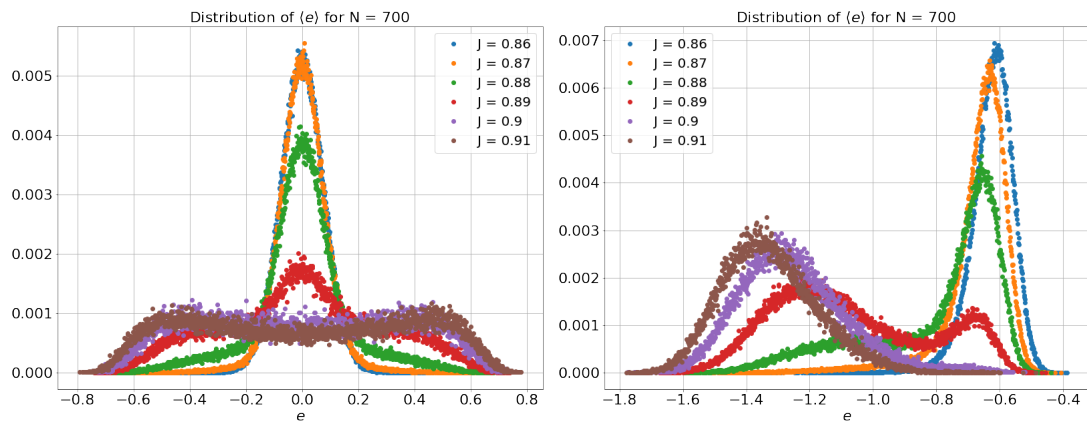Figure 4.15: $h = 0$. Pairs with $N = 700$.

Figure 4.16: $h = 0$.

Bibliography

[1] E.J.J. Van Rensburg. *The Statistical Mechanics of Interacting Walks, Polygons, Animals and Vesicles*. Oxford Lecture Series in Mathe. Oxford University Press, 2015. ISBN: 9780199666577. URL: https://books.google.ru/books?id=LIVMCAAAQBAJ.

[2] "Monte Carlo and Molecular Dynamics Simulations in Polymer Science Edited by Kurt Binder." In: (1995).

[3] Carlo Vanderzande. *Lattice models of polymers*. Cambridge University Press, 1998.

[4] "Statistical Physics". In: *Equilibrium Statistical Physics: Phases of Matter and Phase Transitions*. Ed. by Marc Baus and Carlos F. Tejero. Berlin, Heidelberg: Springer Berlin Heidelberg, 2008, pp. 45–63. ISBN: 978-3-540-74632-4. DOI: 10.1007/978-3-540-74632-4_3. URL: https://doi.org/10.1007/978-3-540-74632-4_3.

[5] Kit Fun Lau and Ken A Dill. "A lattice statistical mechanics model of the conformational and sequence spaces of proteins". In: *Macromolecules* 22.10 (1989), pp. 3986–3997.

[6] Jinfeng Zhang, S. C. Kou, and Jun S. Liu. "Biopolymer structure simulation and optimization via fragment regrowth Monte Carlo". In: *The Journal of Chemical Physics* 126.22 (2007), p. 225101. DOI: 10.1063/1.2736681. eprint: https://doi.org/10.1063/1.2736681. URL: https://doi.org/10.1063/1.2736681.

[7] Hsiao-Ping Hsu et al. "Growth-based optimization algorithm for lattice heteropolymers". In: *Phys. Rev. E* 68 (2 2003), p. 021113. DOI: 10.1103/PhysRevE.68.021113. URL: https://link.aps.org/doi/10.1103/PhysRevE.68.021113.

[8] Robert Helling et al. "The designability of protein structures". In: *Journal of Molecular Graphics and Modelling* 19.1 (2001), pp. 157 –167. ISSN: 1093-3263. DOI: https://doi.org/10.1016/S1093-3263(00)00137-6. URL: http://www.sciencedirect.com/science/article/pii/S1093326300001376.

[9] Kamilla Faizullina and Evgeni Burovski. "Globule-coil transition in the dynamic HP model". In: *Journal of Physics: Conference Series* 1740 (Jan. 2021), p. 012014. ISSN: 1742-6588. DOI: 10.1088/1742-6596/1740/1/012014.

[10] T Garel, H Orland, and E Orlandini. *Phase diagram of magnetic polymers*. 1999, pp. 261–268.

[11] Andrea Papale and Angelo Rosa. "The Ising model in swollen vs. compact polymers: Mean-field approach and computer simulations". In: *European Physical Journal E* 41 (12 Dec. 2018). ISSN: 1292895X. DOI: 10.1140/epje/i2018-11752-2.

[12]   Damien Paul Foster and Debjyoti Majumdar. "Critical behavior of magnetic polymers in two and three dimensions". In: *Phys. Rev. E* 104 (2 2021), p. 024122. DOI: 10.1103/PhysRevE.104.024122. URL: https://link.aps.org/doi/10.1103/PhysRevE.104.024122.

[13]   Kamilla Faizullina, Ilya Pchelintsev, and Evgeni Burovski. "Critical and geometric properties of magnetic polymers across the globule-coil transition". In: *Phys. Rev. E* 104 (5 2021), p. 054501. DOI: 10.1103/PhysRevE.104.054501. URL: https://link.aps.org/doi/10.1103/PhysRevE.104.054501.

[14]   J M Kosterlitz and D J Thouless. "Ordering, metastability and phase transitions in two-dimensional systems". In: *Journal of Physics C: Solid State Physics* 6.7 (1973), pp. 1181–1203. DOI: 10.1088/0022-3719/6/7/010. URL: https://doi.org/10.1088/0022-3719/6/7/010.

[15]   Martin Hasenbusch. "The two-dimensionalXYmodel at the transition temperature: a high-precision Monte Carlo study". In: *Journal of Physics A: Mathematical and General* 38.26 (2005), 5869–5883. ISSN: 1361-6447. DOI: 10.1088/0305-4470/38/26/003. URL: http://dx.doi.org/10.1088/0305-4470/38/26/003.

[16]   Marios Nikolaou. "A Matter of Disorder: Monte Carlo Simulations of Phase Transitions in Strongly Disordered Systems". PhD thesis. KTH, 2007.

[17]   Kurt Binder and Dieter W. Heermann. *Monte Carlo Methods for the Sampling of Free Energy Landscapes*. 2010, pp. 153–174. ISBN: 9783642031625. DOI: 10.1007/978-3-642-03163-2_6.

[18]   Bin Li, Neal Madras, and Alan D Sokal. *Critical Exponents, Hyperscaling, and Universal Amplitude Ratios for Two-and Three-Dimensional Self-Avoiding Walks*. 1995.

[19]   Bertrand Duplantier and Hubert Saleur. *Exact Tricritical Exponents for Polymers at the e Point in Two Dimensions*. 1987.

[20]   Alberto Berretti and Alan D Sokal. "New Monte Carlo method for the self-avoiding walk". In: *Journal of Statistical Physics* 40.3-4 (1985), pp. 483–531.

[21]   Kurt Binder. "Finite size scaling analysis of Ising model block distribution functions". In: *Zeitschrift für Physik B Condensed Matter* 43.2 (1981), pp. 119–140.